3

Application of Monte Carlo Simulation and Voxel Models to Internal Dosimetry

Sakae Kinase, Akram Mohammadi and Masa Takahashi
Japan Atomic Energy Agency
Japan

1. Introduction

There has been a considerable accumulation of usage of voxel models for internal radiation dosimetry (Xu & Eckerman, 2009 ; Zaidi & Tsui, 2009). The human voxel models of the Reference Male and Reference Female have been introduced and used to evaluate the energy deposition in organs resulting from internal radiation exposures by the International Commission on Radiological Protection (ICRP) (ICRP, 2009). Inter-comparisons on Monte Carlo modeling for *in vivo* measurements of radionuclides in knee and torso voxel models were undertaken to upgrade dosimetry programmes in EU (Gomez-Ros, *et al*., 2008; Gualdrini & Ferrari 2008). At the Japan Atomic Energy Agency (JAEA), several studies have been conducted on the use of voxel models for internal dosimetry (Kinase, *et al*., 2003; 2004; 2007a; 2007b; 2008a; 2008b; 2009a; 2009b; Mohammadi & Kinase; Takahashi, *et al*.). Specific absorbed fractions (SAFs) and S values have been evaluated for preclinical assessments of radiopharmaceuticals using human voxel models and a mouse voxel model. Computational calibration of *in vivo* measurement system has been also made using Japanese and Caucasian voxel models, the knee and torso voxel models. In addition, for radiation protection of the environment, absorbed fractions (AFs) have been evaluated using a frog voxel model. Each study has been made by using Monte Carlo simulations. These data by Monte Carlo simulations and voxel models could adequately reproduce those by measurements. Voxel models are significant tools for internal dosimetry since the models are anatomically realistic.

2. Voxel models

The voxel models are based on actual image data obtained from computed tomography, magnetic resonance imaging and cryosections. Hence, the shape of the voxel models is more realistic than for the stylized models such as the Medical Internal Radiation Dose (MIRD) mathematical model (Cristy & Eckerman, 1987). The voxels of tissue are grouped together to form appropriate organ volumes. Every voxel belongs to organ/tissue which is assigned a unique identification number and appropriate attenuation properties which are assumed to be uniform in all voxels within the organ/tissue.

Several voxel models have been used for internal dosimetry at JAEA: the Japanese adult male human "Otoko"(Saito, *et al*., 2001), the Japanese adult female human "Onago"(Saito, *et al*., 2008), the Caucasian adult male human "MAX06"(Kramer, *et al*., 2006), the Caucasian

adult female human "FAX06"(Kramer, *et al*., 2006), ICRP/ICRU reference adult male human "RCP-AM"(ICRP, 2009, Hadid, *et al*., 2010), the male mouse "Digimouse"(Dogdas, *et al*., 2007), and the frog (Kinase, 2008b; 2009b). The frog voxel model, shown in Figure 1, was developed for radiation protection of the environment. The GSF child female human "Child"(Veit, *et al*., 1989)and the MIRD-type voxel models were used for validation of Monte Carlo simulations. In addition, the knee and torso voxel models were used in the inter-comparisons on Monte Carlo modeling for *in vivo* measurements of radionuclides. Table 1 shows the characteristics of the voxel models used at JAEA.

Fig. 1. Image of the frog voxel model.

Name	Image	Organization
Otoko	CT	JAEA
Onago	CT	JAEA
MAX06	CT	Federal University of Pernambuco
FAX06	CT	Federal University of Pernambuco
RCP-AM	CT	ICRP/ICRU
Digimouse	Micro-CT and color cryosection	University of Southern California
frog	Cryosection	JAEA
Child	CT	Helmholtz Zentrum München
MIRD-type	Combinatorial geometry	JAEA
knee	CT	EURADOS/CIEMAT
Livermore torso	CT	EURADOS/IRSN

Table 1. Voxel models with their characteristic.

3. Monte Carlo codes

Two Electron Gamma Shower (EGS) version 4 (Nelson, *et al*., 1985) user codes were developed for internal dosimetry: the UCSAF (Kinase, *et al*. 2003) and UCWBC codes (Kinase, *et al*. 2007b) . Although the EGS4 code is very popular as a general purpose package

for Monte Carlo simulation of the coupled transport of electrons and photons in an arbitrary geometry for particles with energies above a few keV up to several TeV, users have to write complicated geometries such as voxel models in an extended FORTRAN language known as Mortran. It is hard for users to write the geometries accurately. Hence, the UCSAF and UCWBC codes have been developed as packages of subroutines plus model data, and prevents users from writing geometries in Mortran. The UCSAF code is used for evaluations of organ doses from internal radiation exposures, particularly SAF evaluations. The UCWBC code allows accurate *in vivo* measurements of radionuclides in human body. In the UCWBC code, specifications of modeling are also made using the combinatorial geometry (CG) method. Rayleigh scattering, Doppler broadening in Compton scattering, linearly polarized photon scattering and electron impact ionization are included by means of options. The cross–section data for photons are taken from PHOTX (RSIC,1989), and the data for electrons and positrons are taken from ICRU report 37 (ICRU, 1984). The paremeter reduced electron-step transport algorithm (PRESTA) is used to improve the electron transport in the low-energy region.

4. AFs, SAFs, S values and calibration factors

4.1 Absorbed fractions (AFs) and specific absorbed fractions (SAFs)

The absorbed fraction (AF) is the fraction of the energy emitted by source organ that is absorbed in target organ. The AF is a key quantity for evaluating internal organ doses. AFs in organisms from internal sources are evaluated for the protection of the environment.

From the viewpoint of kidney toxicity, self-irradiation AFs for photons and electrons in the kidneys were evaluated for the Otoko, Onago, MAX06, FAX06, RCP-AM, Digimouse and frog voxel models using the UCSAF code. The self-irradiation AFs were calculated by using the energy emitted from the kidneys and energy deposited within the kidneys. Table 2 compares the masses of the kidneys of the voxel models. The sources of photons and electrons were assumed to be monoenergetic in the energy range 10 keV to 4 MeV, uniformly distributed in the kidneys of the voxel models. Photon and electron histories were run at numbers sufficient to reduce statistical uncertainties below 5 %. The transport of photons and electrons had been followed until their energies fell below energy cutoffs of 1 keV for photons and 10 keV for electrons.

To examine suborgan dosimetry for the kidneys, self-irradiation AFs were evaluated for photons and electrons in the kidneys of the RCP-AM voxel model. Since the RCP-AM voxel model has a multiregion model of the kidney that consists of cortex, medulla and pelvis, it allow evaluations of regional kidney doses not previously conducted by the current single-region models. The sources of photons and electrons were assumed to be monoenergetic in the energy range 10 keV to 10 MeV, uniformly distributed in the kidneys of the RCP-AM voxel models.

In addition, to evaluate the interspecies scaling of organ doses from mouse to human, the self-irradiation AFs in the kidneys of the Digimouse voxel model were compared with those of the Otoko voxel model. Interspecies scaling of organ doses is of scientific and practical interest in the evaluation of new radiopharmaceuticals. The interspecies scaling factors were obtained from the ratio of the self-irradiation AFs for the Otoko voxel model to those for the Digimouse voxel model. In the MIRD Pamphlet No. 11, it is noted that the self-irradiation dose from photons with energies above 100 keV appears to be proportional to -2/3 power of the organ mass. Hence, the interspecies scaling factors for photons were corrected by the

cube root of the organ masses. The interspecies scaling factors for photons and electrons can be expressed in equations in the form

$$(\text{Scaling factor})_{\text{Photon}} = \frac{\text{AF}_{\text{human}}}{\text{AF}_{\text{mouse}}\left(\frac{m_{\text{human}}}{m_{\text{mouse}}}\right)^{\frac{1}{3}}} \quad (1)$$

and

$$(\text{Scaling factor})_{\text{Electron}} = \frac{\text{AF}_{\text{human}}}{\text{AF}_{\text{mouse}}}, \quad (2)$$

where *m* is the organ mass.

Self-irradiation specific absorbed fractions (SAFs) for the kidneys in the Child and MIRD-type voxel models were evaluated for validation of Monte Carlo simulations. The self-irradiation SAF was derived as the AF in the kidneys per unit mass of the kidneys.

Name	Kidneys (kg)
Otoko	2.7×10^{-1}
Onago	2.6×10^{-1}
MAX06	3.1×10^{-1}
FAX06	2.8×10^{-1}
RCP-AM	3.1×10^{-1}
left, cortex	1.1×10^{-1}
left, medulla	3.8×10^{-2}
left, pelvis	7.6×10^{-3}
right, cortex	1.1×10^{-1}
right, medulla	3.9×10^{-2}
right, pelvis	7.9×10^{-3}
Digimouse	5.1×10^{-4}
frog	2.2×10^{-4}

Table 2. The kidney masses for the voxel models.

4.2 S values

S value ($\mu Gy/MBq \cdot s$) is mean absorbed dose to a target organ per unit cumulated activity in the source organ. S values are essential for absorbed dose evaluations in the MIRD system.

Nuclides	E_{max} (MeV)	E_{mean} (MeV)
^{18}F	0.634	0.250
^{90}Y	2.281	0.934

Table 3. Maximum E_{max} and mean E_{mean} energies of the beta-rays for ^{18}F and ^{90}Y.

Self-irradiation S values to the kidneys from uniformly distributed beta-ray emitters within the kidneys were evaluated for the Otoko, Onago, MAX06, FAX06, RCP-AM, Digimouse and frog voxel models. The beta-ray emitters were ^{18}F and ^{90}Y of potential interest in the kidney dosimetry. Table 3 shows the maximum and mean energies for ^{18}F and ^{90}Y. To

evaluate the self-irradiation S values, the total energies deposited in the kidneys per source particles were calculated using the UCSAF code.

4.3 *In vivo* measurements

Whole-body counters are commonly used in radiation protection to identify unintended intakes of radioactive material and assess the radiation exposure to the individual. Calibration methods of whole-body counters using Monte Carlo simulations and voxel models are of considerable practical significance in order to obtain calibration data such as counting efficiencies applicable to a given subject.

Counting efficiencies of a whole-body counter installed at JAEA were evaluated for the Otoko and MAX06 voxel models by the UCWBC code. Figure 2 shows the geometry of the simulation model of the JAEA whole-body counter and MAX06 voxel model. The model was accurately constructed to represent the actual whole-body counter, which has three p-type closed-ended coaxial high purity germanium (HPGe) semiconductor detectors. The crystal of the detector is 73.2 mm in diameter and 85.8 mm in length. The apparent dead layer thickness on the outer surface of the Ge semi-conductor crystal is 0.9 mm. The peak efficiency, relative to that of a 76.2 mm diameter×76.2 mm thick NaI(Tl) crystal, is 80 %, measured for 1,332 keV photons from a source of ^{60}Co at 250 mm. The whole-body counter has a shielding that consists of a room with 2,500 (height) ×2,000 (width) ×2,500 (length) mm^3 internal dimensions and a 200 mm thick wall of steel. The inner side of the room is lined with 3 mm of lead, 1mm of copper and faced plastic wall. The counting efficiencies were evaluated by dividing the number of photons that deposited all initial energy in the detectors, by the number of simulated histories. The photon sources were assumed to be isotropic, and to be homogeneously distributed within the voxel models.

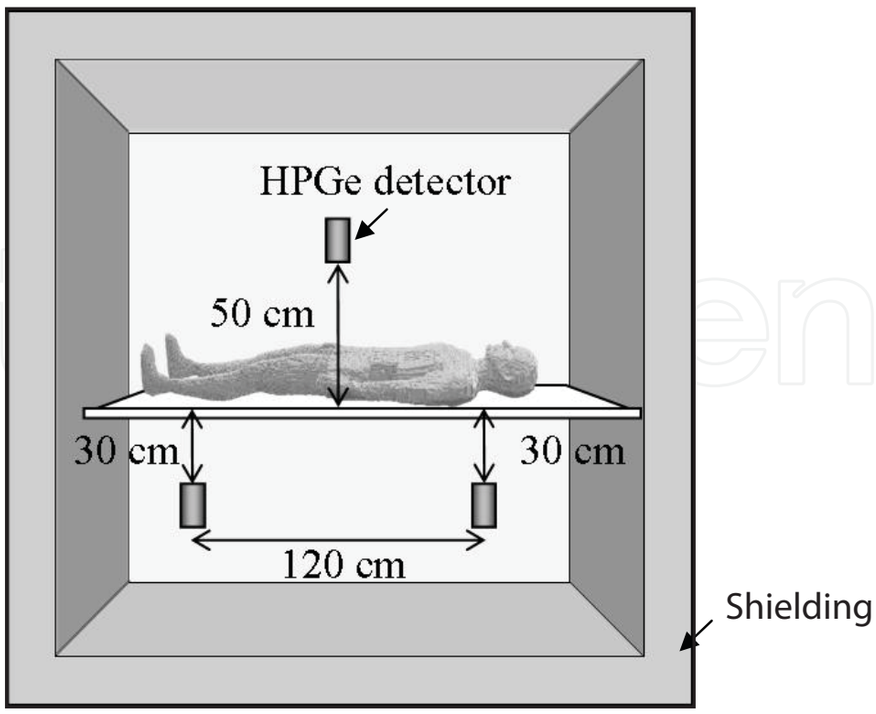

Fig. 2. Geometric model of the whole-body counter and the MAX06 voxel model.

In addition, counting efficiencies of the whole-body counter were evaluated for heterogeneous distributions of radionuclides, ^{137}Cs in the MAX06 voxel model. The radionuclide distributions were derived from the biokinetic models provided by the ICRP. The biokinetic models include transfer of the intake radionuclides from inhalation to excretion. Radioactivities differing with time in compartments that indicate separated organs are expressed as first-order kinetics. A single intake of ^{137}Cs by inhalation was assumed. The absorption types for the respiratory tract organs were assumed to be type F for ^{137}Cs. The Activity Median Aerodynamic Diameter (AMAD) was 5 μm. To assess the influence of radionuclide distributions within the MAX06 voxel model on whole-body counting, the counting efficiencies for heterogenous distributions were compared with those for homogenous distributions.

4.4 Inter-comparison on *in vivo* measurements

In recent years, two inter-comparisons on *in vivo* measurements have been conducted in EU. The "International comparison on Monte Carlo modeling for *in vivo* measurement of Americium in a knee phantom" was organized within the EU Coordinated Action CONRAD (Coordinated Network for Radiation Dosimetry) as a joint initiative of EURADOS working groups 6 and 7. The "International comparison on Monte Carlo modelling for *in vivo* measurement of Enriched Uranium in the lungs of a Livermore phantom" has been carried out as an EURADOS working groups 6 and 7 joint collaboration.

Response function of a detection system consisting of a pair of Low Energy (LE) Ge semi-conductor detectors was evaluated for ^{241}Am in the knee voxel model by the UCWBC code. A ^{241}Am source was assumed to be homogeneously distributed in the bone of the knee voxel model. Each LE Ge detector contains a germanium crystal 70mm in diameter and 25mm in thickness. An entrance window made of carbon fibre and epoxy resin of thickness 0.6mm is separated from the Ge crystal by a 5mm vacuum gap. The response function was folded with Gaussian distributions, since the effects of fluctuation in the signal of the detector are not considered in the UCWBC code.

Response functions of the four LE Ge semi-conductor detector system were evaluated for enriched uranium (^{234}U, ^{235}U and ^{238}U) in lungs of a torso voxel model, namely the Livermore voxel model. Two tasks were challenged: lung counting simulations with the torso voxel model without extra-thoracic plate and one with plate.

5. Applications for internal dosimetry

5.1 AFs

Figure 3 shows the self-irradiation AFs for photons in the kidneys of the Otoko, Onago, MAX06, FAX06, RCP-AM, Digimouse and frog voxel models in the energy range from 10 keV to 4 MeV. The self-irradiation AFs depend on the photon energy and decrease with an increase in photon energy on the whole. These results indicate that the self-irradiation AFs for the Digimouse and frog voxel models exhibit large deviations from those for the human voxel models in the high-energy region. This is mainly due to the different shape and size of the kidneys. The self-irradiation AFs for kidneys depend on the organ mass.

The self-irradiation AFs for electrons in the kidneys of the Otoko, Onago, MAX06, FAX06, RCP-AM, Digimouse and frog voxel models are shown in Figure 4. These finding leads to a conclusion that the self-irradiation AFs for the voxel models are almost unity in the electron energy range from 10 keV to 100 keV and that the self-irradiation AFs for the Digimouse

and frog voxel models are inconsistent with those for the human voxel models in the higher energy region. The apparent inconsistency is attributed to the different size of the kidneys. The electrons with energy 4 MeV (csda range 2.0 g/cm^2) are not always absorbed within the kidneys of the Digimouse and frog voxel models.

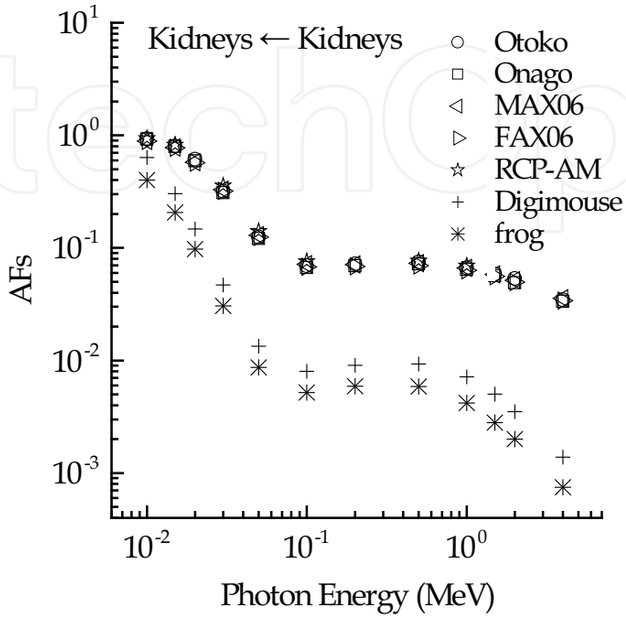

Fig. 3. Self-irradiation AFs for the >Kidneys in the Otoko, Onago, MAX06, FAX06, RCP-AM, Digimouse and frog voxel models in the photon energy 10keV-4MeV.

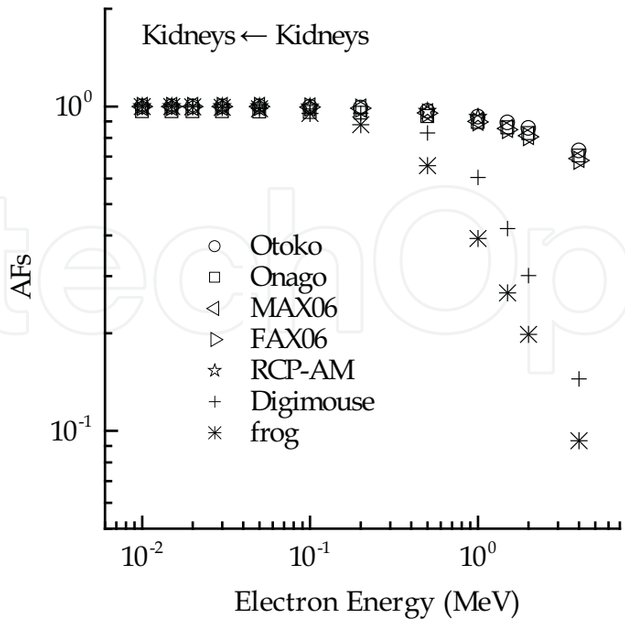

Fig. 4. Self-irradiation AFs in the Kidneys for the Otoko, Onago, MAX06, FAX06, RCP-AM, Digimouse and frog voxel models in the electron energy 10keV-4MeV.

The self-irradiation AFs in the regional kidney of the RCP-AM voxel model are listed in Tables 4 and 5. The self-irradiation AFs for photons decrease with an increase in energy. The self-irradiation AFs for electrons remain unchanged up to around 1 MeV, above which they decrease abruptly. This result is consistent with the self-irradiation AFs in the whole kidneys. The self-irradiation AFs for electrons up to around 1 MeV are in accord with the ratio of the mass of the regional kidney to the mass of the whole kidneys. The self-irradiation AFs for photons and electrons in the left kidney are lower than those in the right kidney. As mentioned in the previous studies, this is due to the different size of each kidney.

Energy (MeV)	left, cortex	left, medulla	left, pelvis	right, cortex	right, medulla	right, pelvis
0.01	3.2×10^{-1}	1.2×10^{-1}	2.4×10^{-2}	3.3×10^{-1}	1.3×10^{-1}	2.5×10^{-2}
0.015	2.7×10^{-1}	1.1×10^{-1}	2.3×10^{-2}	2.8×10^{-1}	1.2×10^{-1}	2.4×10^{-2}
0.03	1.1×10^{-1}	5.1×10^{-2}	1.1×10^{-2}	1.2×10^{-1}	5.3×10^{-2}	1.1×10^{-2}
0.05	4.4×10^{-2}	2.0×10^{-2}	4.0×10^{-3}	4.7×10^{-2}	2.1×10^{-2}	4.4×10^{-3}
0.06	3.4×10^{-2}	1.5×10^{-2}	3.1×10^{-3}	3.6×10^{-2}	1.6×10^{-2}	3.4×10^{-3}
0.08	2.6×10^{-2}	1.2×10^{-2}	2.4×10^{-3}	2.8×10^{-2}	1.2×10^{-2}	2.6×10^{-3}
0.1	2.4×10^{-2}	1.1×10^{-2}	2.2×10^{-3}	2.6×10^{-2}	1.1×10^{-2}	2.4×10^{-3}
0.3	2.4×10^{-2}	1.1×10^{-2}	2.2×10^{-3}	2.6×10^{-2}	1.1×10^{-2}	2.4×10^{-3}
0.5	2.4×10^{-2}	1.1×10^{-2}	2.2×10^{-3}	2.6×10^{-2}	1.1×10^{-2}	2.4×10^{-3}
0.8	2.3×10^{-2}	1.0×10^{-2}	2.1×10^{-3}	2.4×10^{-2}	1.1×10^{-2}	2.3×10^{-3}
1	2.2×10^{-2}	9.8×10^{-3}	2.0×10^{-3}	2.3×10^{-2}	1.0×10^{-2}	2.2×10^{-3}
3	1.4×10^{-2}	6.3×10^{-3}	1.3×10^{-3}	1.5×10^{-2}	6.7×10^{-3}	1.4×10^{-3}
6	8.8×10^{-3}	4.0×10^{-3}	8.3×10^{-4}	9.6×10^{-3}	4.2×10^{-3}	9.1×10^{-4}
8	7.1×10^{-3}	3.1×10^{-3}	6.5×10^{-4}	7.7×10^{-3}	3.3×10^{-3}	7.1×10^{-4}
10	6.0×10^{-3}	2.6×10^{-3}	5.3×10^{-4}	6.5×10^{-3}	2.7×10^{-3}	5.8×10^{-4}

Table 4. Self-irradiation AFs for photons in the kidneys of the RCP-AM voxel models.

Energy (MeV)	left, cortex	left, medulla	left, pelvis	right, cortex	right, medulla	right, pelvis
0.01	3.5×10^{-1}	1.2×10^{-1}	2.5×10^{-2}	3.5×10^{-1}	1.3×10^{-1}	2.5×10^{-2}
0.015	3.5×10^{-1}	1.2×10^{-1}	2.5×10^{-2}	3.5×10^{-1}	1.3×10^{-1}	2.5×10^{-2}
0.03	3.5×10^{-1}	1.2×10^{-1}	2.5×10^{-2}	3.5×10^{-1}	1.3×10^{-1}	2.5×10^{-2}
0.05	3.5×10^{-1}	1.2×10^{-1}	2.5×10^{-2}	3.5×10^{-1}	1.3×10^{-1}	2.5×10^{-2}
0.06	3.4×10^{-1}	1.2×10^{-1}	2.5×10^{-2}	3.5×10^{-1}	1.3×10^{-1}	2.5×10^{-2}
0.08	3.4×10^{-1}	1.2×10^{-1}	2.5×10^{-2}	3.5×10^{-1}	1.3×10^{-1}	2.5×10^{-2}
0.1	3.4×10^{-1}	1.2×10^{-1}	2.5×10^{-2}	3.5×10^{-1}	1.3×10^{-1}	2.5×10^{-2}
0.3	3.4×10^{-1}	1.2×10^{-1}	2.5×10^{-2}	3.5×10^{-1}	1.3×10^{-1}	2.5×10^{-2}
0.5	3.3×10^{-1}	1.2×10^{-1}	2.4×10^{-2}	3.4×10^{-1}	1.3×10^{-1}	2.5×10^{-2}
0.8	3.2×10^{-1}	1.2×10^{-1}	2.4×10^{-2}	3.3×10^{-1}	1.3×10^{-1}	2.5×10^{-2}
1	3.1×10^{-1}	1.2×10^{-1}	2.4×10^{-2}	3.2×10^{-1}	1.3×10^{-1}	2.5×10^{-2}
3	2.5×10^{-1}	1.1×10^{-1}	2.2×10^{-2}	2.6×10^{-1}	1.2×10^{-1}	2.4×10^{-2}
6	1.9×10^{-1}	9.2×10^{-2}	1.9×10^{-2}	2.0×10^{-1}	9.7×10^{-2}	2.1×10^{-2}
8	1.6×10^{-1}	7.7×10^{-2}	1.6×10^{-2}	1.7×10^{-1}	8.1×10^{-2}	1.7×10^{-2}
10	1.4×10^{-1}	6.4×10^{-2}	1.3×10^{-2}	1.5×10^{-1}	6.8×10^{-2}	1.5×10^{-2}

Table 5. Self-irradiation AFs for electrons in the kidneys of the RCP-AM voxel models.

The interspecies scaling factors of self-irradiation doses for the kidneys from the Digimouse voxel model to the Otoko voxel model are plotted against radiation energy in Figure 5. The interspecies scaling factors, which decrease with an increase in organ mass, show energy dependence. The photon scaling factors are close to unity in the energy range from 50 keV to 500 keV. The electron scaling factors are also close to unity in the energy range from 10 keV to 200 keV. The important finding is that the scaling factor for the photon self-irradiation AF, which is corrected by the cube root of the organ mass, shows the similar trend as a function of energy with the scaling factor for the electron self-irradiation AF.

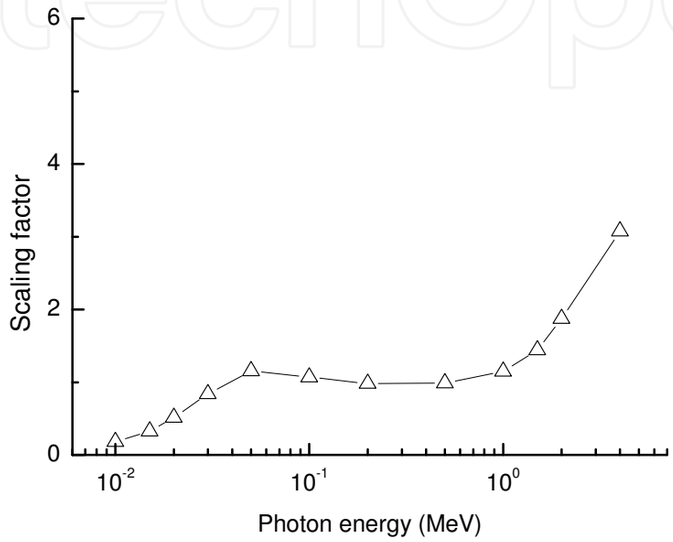

(a) Photon

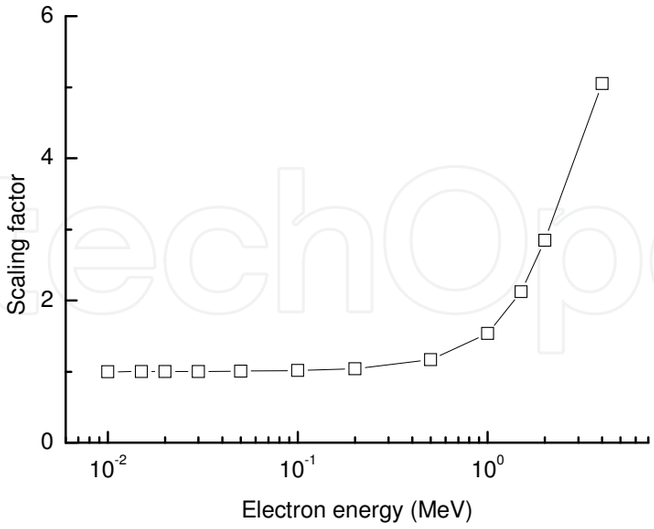

(b) Electron

Fig. 5. Interspecies scaling factors of self-irradiation doses for the kidneys from the Digimouse voxel model to the Otoko voxel model in the energy 10keV-4MeV. (a) Photon, (b) Electron.

5.2 SAFs

The self-irradiation SAFs in the Child voxel model were evaluated by the UCSAF code considering energy deposition due to secondary electrons. Table 6 shows the results in comparison with the SAFs obtained at GSF, in which the kerma approximation -SAFs calculated by considering the energy to be deposited at the point of photon interaction- has been used. The SAFs by the UCSAF code under kerma approximation agree with the GSF data. The statistical uncertainty for the SAF at the worst case was 4.0 %. Consequently, the above results substantiated that the UCSAF code can be used to calculate SAFs. The SAF considering secondary electrons induced by photons is about 0.75 times that by the kerma approximation for photon energy 4 MeV. The discrepancy is due to different energy deposition within the volume of interest due to the removal of energy by the secondary electrons within the kidneys. It may be deduced that SAFs for target tissues that are also the source evaluated by the kerma approximation are appropriate in the photon energy of 10 keV to 1 MeV and not in the photon energy of several MeV.

Self-irradiation SAFs for the kidneys in the MIRD-type voxel models are also shown in Table 6. The SAFs by the UCSAF code are in good agreement with those evaluated in ORNL. The SAFs by the UCSAF code exhibits slightly deviations from the ORNL data in the photon energy above 1 MeV. It is attributable to the treatment of secondary electrons.

Energy (MeV)	Child			MIRD	
	Electron transport	Kerma	GSF Kerma	Electron transport	ORNL Kerma
0.01	4.9	4.9		3.1	3.1
0.015	4.1	4.1		2.7	2.6
0.02	3.1	3.1	3.2	2.0	2.0
0.03	1.6	1.6	1.7	1.1	9.9×10^{-1}
0.05	5.9×10^{-1}	5.9×10^{-1}	6.3×10^{-1}	4.1×10^{-1}	4.0×10^{-1}
0.1	3.3×10^{-1}	3.3×10^{-1}	3.4×10^{-1}	2.3×10^{-1}	2.3×10^{-1}
0.2	3.4×10^{-1}	3.4×10^{-1}	3.4×10^{-1}	2.4×10^{-1}	2.4×10^{-1}
0.5	3.5×10^{-1}	3.6×10^{-1}	3.6×10^{-1}	2.5×10^{-1}	2.5×10^{-1}
1	3.2×10^{-1}	3.3×10^{-1}	3.3×10^{-1}	2.2×10^{-1}	2.3×10^{-1}
1.5	2.8×10^{-1}	3.0×10^{-1}	3.0×10^{-1}	2.0×10^{-1}	2.1×10^{-1}
2	2.5×10^{-1}	2.8×10^{-1}	2.8×10^{-1}	1.7×10^{-1}	2.0×10^{-1}
4	1.7×10^{-1}	2.2×10^{-1}	2.5×10^{-1}	1.2×10^{-1}	1.6×10^{-1}

Table 6. Comparison of self-irradiation SAFs in the kidneys of the Child/MIRD-type voxel models between those evaluated by the UCSAF code and those evaluated in GSF/ORNL.

5.3 S values

Figure 6 shows the self-irradiation S values for the kidneys of the Otoko, Onago, MAX06, FAX06, RCP-AM, Digimouse and frog voxel models, for ^{18}F and ^{90}Y. It can be seen that the self-irradiation S values for the small voxel models are much larger than those for the large voxel models.

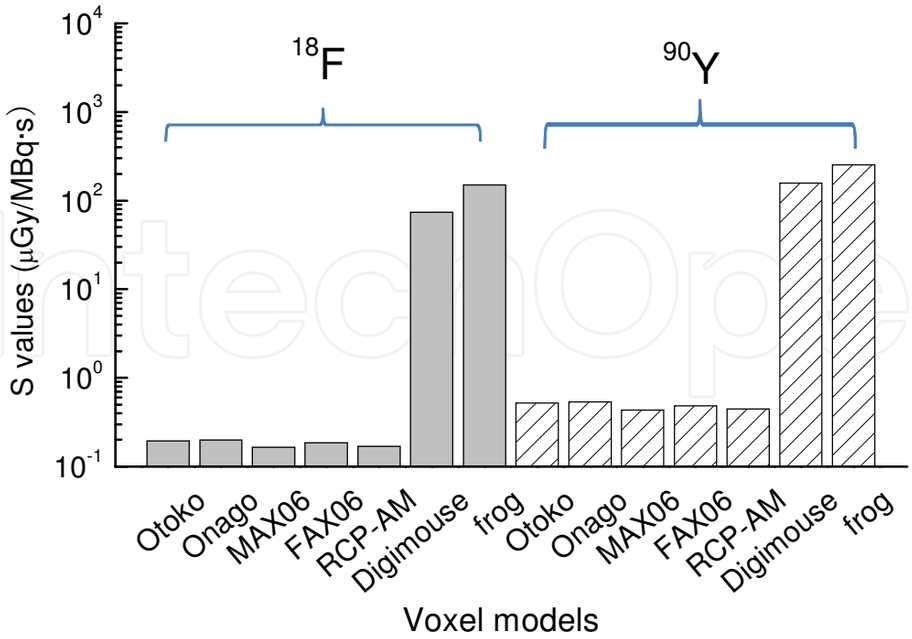

Fig. 6. Self-irradiation S values for ^{18}F and ^{90}Y in the kidneys of the Otoko, Onago, MAX06, FAX06, RCP-AM, Digimouse and frog voxel models.

5.4 Counting efficiencies of a whole-body counter

Figure 7 shows the counting efficiencies of the JAEA whole-body counter for the Otoko and MAX06 voxel models. The counting efficiencies for the Otoko voxel model are slightly larger than those for the MAX06 voxel model over the whole energy range. This is due to geometric differences between the two models.

Table 7 shows the fractions of activity in the organ to total residual amounts in body at 0.5, 3, 10 and 365 days after single intake of ^{137}Cs. The activity of the whole body was defined as sums of those in the blood and total body compartments. At 0.5 days, nasal passage becomes a major source organ because of the entrance compartment for the inhaled material.

Organ	Time after intake (day)			
	0.5	3	10	365
Whole body	68	96	100	100
Nasal passage	32	4		

Table 7. Fractions (%) of ^{137}Cs in organs to total residual amounts.

Figure 8 shows the counting efficiencies for 662 keV photons from ^{137}Cs in the MAX06 voxel model. From the figure, it can be stated that the counting efficiency decreases by 20 % compared with that for the homogenous distribution at 0.5 days after an intake. However, the counting efficiencies do not depend on elapsed times following several days of intake since ^{137}Cs are distributed throughout all organs and tissues of the whole body at 3 days after single intake.

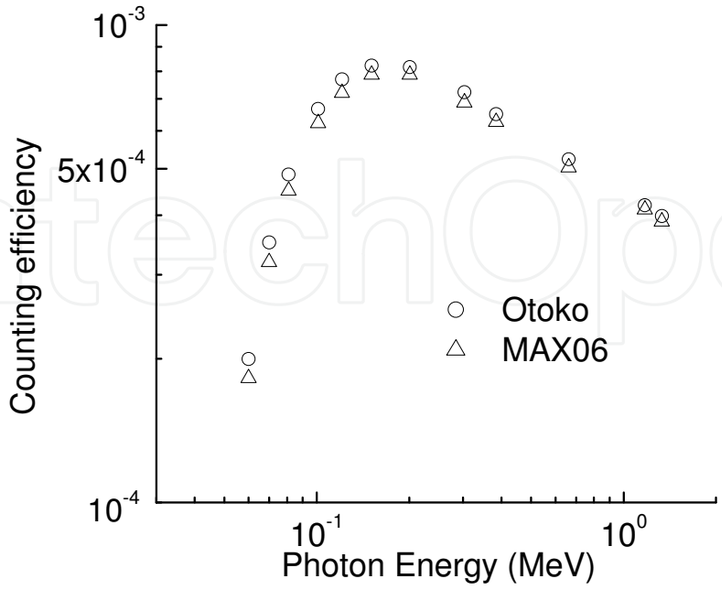

Fig. 7. Comparison of the counting efficiencies for the Otoko voxel model and those for the MAX06 voxel model.

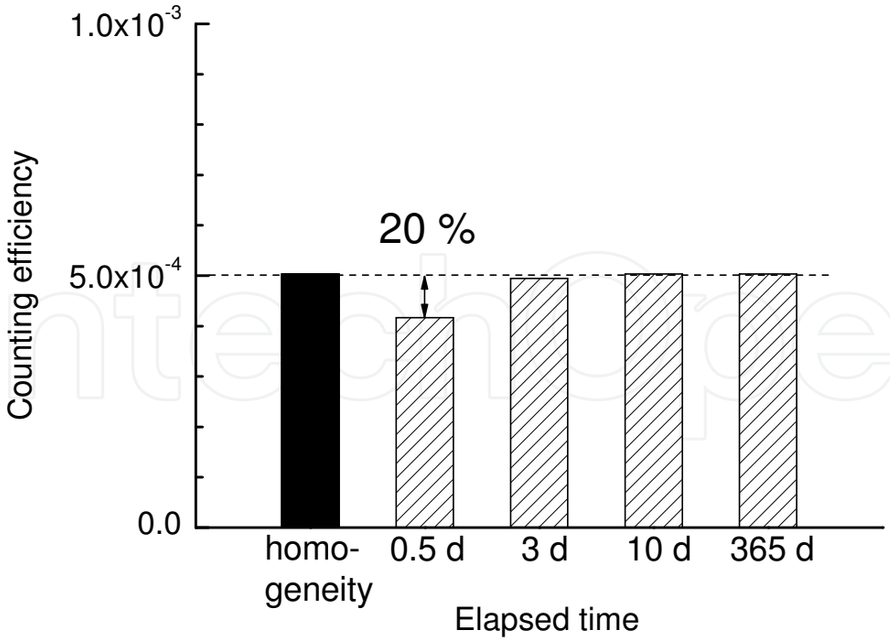

Fig. 8. Counting efficiencies for ^{137}Cs with homogeneous and heterogeneous distributions in the MAX06 voxel model at the elapsed times of 0.5, 3, 10 and 365 days after an intake.

5.5 Inter-comparison

Figure 9 shows calculated and measured response functions of the LE Ge semiconductor detectors for ^{241}Am source in the knee voxel model. These results are consistent with the measurements. It was found that the calculated results represent all important interactions that take place within the LE Ge semiconductor detectors. The response function between the Compton edges (11.3 keV) and the back-scatter peaks (48.2 keV) and X-ray escape peaks (Ge : 11 keV) is reproduced by the calculations. The slight deviation of the calculation from the mesurement in Figure 9 are considered to be due to having no regard for the directional dependence of peak positions in the calculations. From the figures, it can be stated that the calibration data by the UCWBC codes can adequately reproduce those by measurements.

Figure 10 shows calculated response functions of the LE Ge semiconductor detectors for uranium source in the torso voxel model. There is significant difference in the response functions for torso voxel model between with and without plate. The difference is attributed to the attenuations of photons from the lungs in the plate. The response function is reproduced by the calculations.

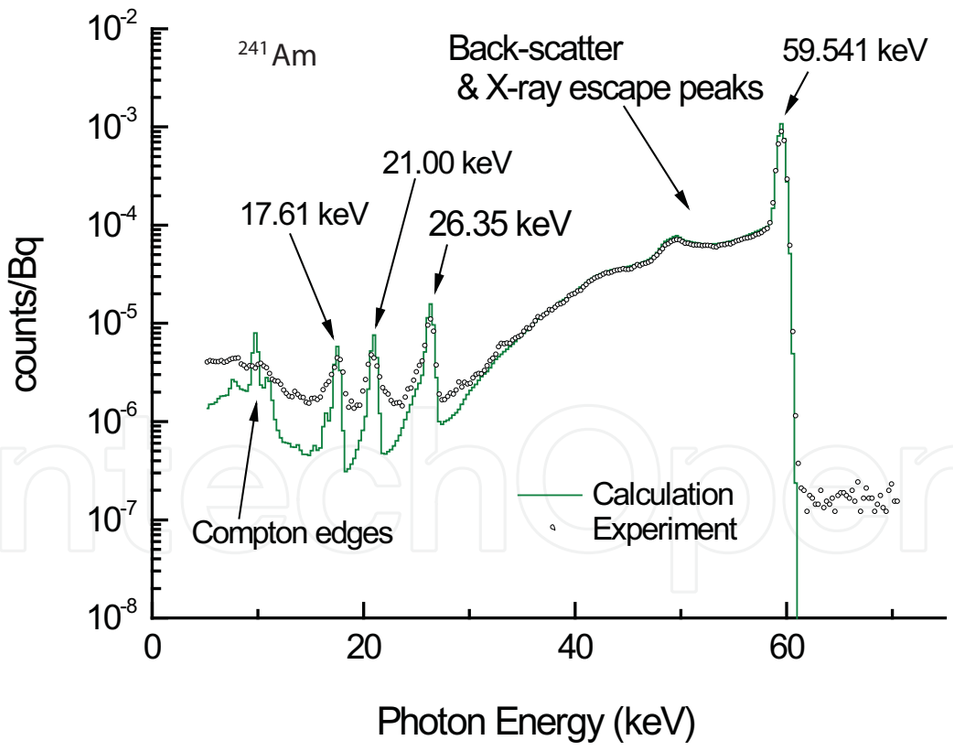

Fig. 9. Comparison of the measured and calculated response functions for the knee voxel model.

6. Conclusion

Monte Carlo simulations and voxel models were found to be significant tools for internal dosimetry. In particular, voxel models were confirmed to be useful for internal organ dose evaluations since they are anatomically realistic. This fact indicates that several studies on correction of the *in vivo* measurement efficiency for the variability of human subjects and interspecies scaling of organ doses will succeed.

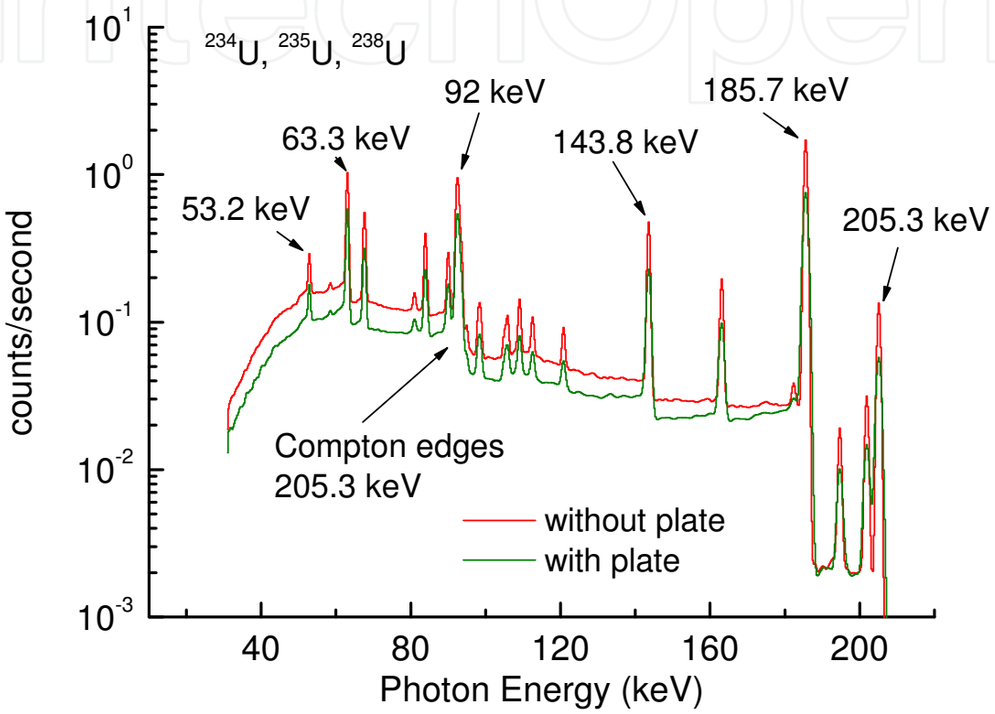

Fig. 10. Response functions of the LE Ge semiconductor detectors for uranium source in the Livermore torso voxel model.

7. References

Cristy, M. & Eckerman, K. (1987). Specific absorbed fractions of energy at various ages from internal photon sources, ORNL/TM-8381 (Oak Ridge, TN :Oak Ridge National Laboratory).

Dogdas, B., Stout, D., Chatziioannou, A. F., *et al.* (2007). Digimouse: a 3D whole body mouse atlas from CT and cryosection data. *Phys. Med. Biol.* 52, 577-587.

Gomez-Ros, J. M., de Carlan, L., Franck, D., *et al.* (2008). Monte Calro modelling of Germanium detectors for the measurement of low energy photons in internal dosimetry: results of an international comparison, *Radiat. Meas.* 43, 510-515.

Gualdrini, G. & Ferrari, P. (2008). *Proceedings of the International workshop on uncertainty assessment in computational dosimetry,* ISBN 978-3-9805741-9-8, Bologna, October 2007, EURADOS.

Hadid, L., Desbree, A., Schlattl, H. *et al.* (2010). Application of the ICRP/ICRU reference computational phantoms to internal dosimetry: calculation of specific absorbed fractions of energy for photons and electrons, *Phys. Med. Biol.*, 55, 3631-3641.

ICRP (2009a). Adult reference computational phantoms, ICRP Publication 110.

ICRP (2009b). Environmental protection: the concept and use of reference animals and plants, ICRP Publication 108.

ICRU (1984). Stopping powers for electrons and positrons. ICRU Report 37.

Kinase, S., Zankl, M., Kuwabara, J., *et al.* (2003). Evaluation of specific absorbed fractions in voxel phantoms using Monte Carlo simulation *Radiat. Prot. Dosim.*, 105, 557-563.

Kinase, S., Zankl, M., Funabiki, J., *et al.* (2004). Evaluation of S values for beta-ray emitters within the urinary bladder, *J. Nucl. Sci. Technol. Suppl.*4, 125, 136-139.

Kinase, S. & Saito, K. (2007a). Evaluation of self-dose S values for positron emitters in voxel phantoms, *Radiat. Prot. Dosim.*, 127, 197-200.

Kinase, S., Takagi, S., Noguchi, H., *et al.* (2007b). Application of voxel phantoms and Monte Carlo method to whole-body counter calibration, *Radiat. Prot. Dosim.*, 125, 189-193.

Kinase, S., Takahashi, M. & Saito, K. (2008a). Evaluation of self-absorbed doses for the kidneys of a voxel mouse, *J. Nucl. Sci. Technol. Suppl.*5, 268-270.

Kinase, S. (2008b). Voxel-based frog phantom for internal dose evaluation, *J. Nucl. Sci. Technol*. 45, 1049-1052.

Kinase, S., Matsuhashi, S. & Saito, K. (2009a). Inter-species scaling of self-organ doses from a voxel mouse to voxel humans, *Nucl. Technol.*, 168, 154-157.

Kinase, S. (2009b). Monte Carlo simulations of photon absorbed fractions in a frog voxel phantom, *Proc. IEEE* 97, 2086-2097.

Kramer, R., Khoury, H. J., Vieira, J. W., *et al.* (2006). MAX06 and FAX06: update of two adult human phantoms for radiation protection dosimetry, *Phys. Med. Biol.*, 51, 3331-3346.

Mohammadi, A. & Kinase, S. Monte Carlo simulation of photon specific absorbed fractions in a mouse voxel phantom, *Prog. Nucl. Sci. Technol.* (in press).

Nelson, W. R., Hirayama, H., Rogers, D. W. O. (1985). The EGS4 code system, *SLAC-265*.

RSIC (1989). DLC-136/PHOTX Photon interaction cross section library (contributed by National institute of standards and technology)

Saito, K., Wittmann, A., Koga, S., *et al.* (2001). Construction of a computed tomographic phantom for a Japanese male adult and dose calculation System, *Radiat. Environ. Biophys*. 40, 69-76.

Saito, K., Koga, S., Ida, Y., *et al.* (2008). Construction of a voxel phantom based on CT data for a Japanese female adult and its use for calculation of organ doses from external electrons. *Jpn. J. Health Phys.*, 43, 122-130.

Takahashi, M., Kinase, S. & Kramer, R. Evaluation of counting efficiencies of whole-body counter using Monte Carlo simulation with voxel phantoms. *Radiat. Prot. Dosim.* (in press).

Veit, R., Zankl, M., Petoussi, N., *et al.* (1989). Tomographic anthropomorphic models: part 1, GSF-Bericht 3/89 Neuherberg, Germany.

Xu, X. G. & Eckerman, K. F. (2009). *Handbook of Anatomical Models for Radiation Dosimetry,* CRC Press, ISBN 978-1-4200-5979-3, New York.

Zaidi, H. & Tsui, B. M. W. (2009)., Review of computational anthropomorphic anatomical and physiological models, *Proc. IEEE* 97, 1938-1953.

Applications of Monte Carlo Methods in Biology, Medicine and Other Fields of Science

Edited by Prof. Charles J. Mode

ISBN 978-953-307-427-6
Hard cover, 424 pages
Publisher InTech
Published online 28, February, 2011
Published in print edition February, 2011

This volume is an eclectic mix of applications of Monte Carlo methods in many fields of research should not be surprising, because of the ubiquitous use of these methods in many fields of human endeavor. In an attempt to focus attention on a manageable set of applications, the main thrust of this book is to emphasize applications of Monte Carlo simulation methods in biology and medicine.

How to reference

In order to correctly reference this scholarly work, feel free to copy and paste the following:

Sakae Kinase, Akram Mohammadi and Masa Takahashi (2011). Application of Monte Carlo Simulation and Voxel Models to Internal Dosimetry, Applications of Monte Carlo Methods in Biology, Medicine and Other Fields of Science, Prof. Charles J. Mode (Ed.), ISBN: 978-953-307-427-6, InTech, Available from: http://www.intechopen.com/books/applications-of-monte-carlo-methods-in-biology-medicine-and-other-fields-of-science/application-of-monte-carlo-simulation-and-voxel-models-to-internal-dosimetry

INTECH
open science | open minds

InTech Europe
University Campus STeP Ri
Slavka Krautzeka 83/A
51000 Rijeka, Croatia
Phone: +385 (51) 770 447
Fax: +385 (51) 686 166
www.intechopen.com

InTech China
Unit 405, Office Block, Hotel Equatorial Shanghai
No.65, Yan An Road (West), Shanghai, 200040, China
中国上海市延安西路65号上海国际贵都大饭店办公楼405单元
Phone: +86-21-62489820
Fax: +86-21-62489821

IntechOpen